

Integration of Enzyme Immobilised Single-walled Carbon Nanotube Arrays into Microchannels for Glucose Detection

Jingxian Yu^{1,3*}, Sinéad M Matthews², Kamran Yunus², Joseph G Shapter¹ and Adrian C Fisher²

¹ School of Chemical and Physical Sciences, Flinders University, Sturt Road, Bedford Park, South Australia 5042, Australia

² Department of Chemical Engineering and Biotechnology, University of Cambridge, New Museums Site, Pembroke Street, Cambridge CB2 3RA, UK

³ School of Chemistry and Physics, The University of Adelaide, Adelaide 5005, Australia

*E-mail: Jingxian.Yu@adelaide.edu.au

Received: 30 December 2012 / Accepted: 17 January 2013 / Published: 1 February 2013

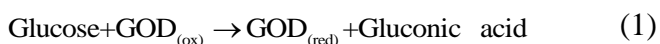
Microfluidic devices for glucose detection have been constructed and developed by integration of covalently immobilised single-walled carbon nanotube arrays functionalised with glucose oxidase into a poly (dimethylsiloxane)-based microfluidic channel. With biocompatible ferrocenecarboxylic acid as electron transfer mediator, these microfluidic devices were tested systematically for electrochemical glucose detection by changing some geometrical parameters such as the width of detecting electrode as well as electrode gap between the enzyme electrode and the detecting electrode. Numerical simulations were also carried out using a finite difference model and used to further understand the concentration profiles in microchannels. The experimental results showed that glucose can be detected with a linear response up to a concentration of 5 mmol L⁻¹. Compared to reported glucose detection techniques, our microfluidic devices have some advantages such as simple design, repeated use and low cost.

Keywords: Microfluidic devices; glucose oxidase; carbon nanotube arrays; glucose detection; ferrocenecarboxylic acid

1. INTRODUCTION

Glucose sensing is extremely important commercially since diabetics need to keep control of their blood glucose to prevent either hypoglycaemia or hyperglycaemia. The increasing prevalence of diabetes in the western world due to lifestyle choices will mean that testing of blood glucose will only increase in importance. Blood glucose should range between 4 and 7 mmol L⁻¹ in healthy humans [1]. The early sensors tested for ketones in urine [2], however the delay in metabolism of glucose to ketone metabolites prevented close monitoring of blood glucose. The big advance in direct measurement of blood glucose came in the late of 1980's, when the enzyme glucose oxidase (GOD) became widely

available [3-5]. GOD oxidises glucose to gluconic acid and liberates hydrogen peroxide, which can then be electrochemically [6] and optically [7] detected. The major problem using the hydrogen peroxide reduction current as an indirect measure of glucose concentration is that oxygen concentration can vary in different samples, providing a large error in measurements. The solution to the problem of variable oxygen concentration was to realise that oxygen only acts as an electron shuttle, removing electrons from the reduced form of GOD and taking them to the electrode [8-10]. This problem could be bypassed by providing an artificial electron shuttle [11]. It has been found that ferrocene and ferrocene derivatives (Fc) have good biocompatibility with GOD [12-15]. They do not denature GOD and access the free electron within the reduced GOD [16, 17]. The glucose detection scheme can be expressed as follows [13]:



Microfluidic techniques offer a number of technical advantages due their ability to manipulate small volumes (10^{-9} to 10^{-18} litres) via channels with dimensions of tens to hundreds of micrometres [18-24]. One of the key challenges is to immobilise reagents and catalysts within these devices providing improved stability and higher sensitivity in chemical analysis [7]. With their large aspect ratio, good chemical stability and their ability to act as near-perfect conductors of electrons, carbon nanotubes have been used as molecular wires for nanoscale electronics and biosensors [4, 25, 26]. Schulz and co-workers [27] reported that highly aligned multi-wall carbon nanotubes synthesised in the shape of towers were embedded into fluidic channels as electrodes for impedance measurement of LNCaP human prostate cancer cells. Preliminary electrochemical impedance spectroscopy results using deionised water, buffer solution, and LNCaP prostate cancer cells showed that nanotube electrodes can distinguish the different solutions and could be used in future cell-based biosensor development. Lee and co-workers [7] reported a simple approach to fabricating a co-enzyme-immobilised mass of single-walled carbon nanotubes (SWCNTs) that has a specific microscale shape by integrating the mass into a poly(dimethylsiloxane) (PDMS)-based microfluidic channel. This microfluidic device was tested for the spectroscopic glucose-detection, and the results showed that the glucose can be detected linearly (in log scale) in a wide range of glucose concentrations. Moreover, microfluidic devices using carbon nanotube materials for the analysis of selected analyte groups of significance in foods such as dietary antioxidants, water-soluble vitamins, vanilla flavors, and isoflavones involved in representative food samples have been explored [28]. Resolution was improved by a factor of 2, and sensitivity was dramatically enhanced with amplification factors toward calibration slopes from 4- to 16-fold. However the traditional approach to fabricating an enzyme/carbon nanotube electrode involves depositing an enzyme layer (commonly composed of an enzyme immobilised within a polymer matrix) over the surface of an electrode resulting in an unknown spatial relationship between the redox proteins and the nanotubes [26, 29].

Vertically aligned carbon nanotube arrays can be coupled with enzymes to provide a favorable surface orientation and act as an electrical connector between their redox centre and the electrode surface [29-33]. Willner's group [31] demonstrated that aligned reconstituted glucose oxidase on the edge of single-wall carbon nanotubes can be linked to an electrode surface. Such enzyme reconstitution on the end of carbon nanotube represents an extremely efficient approach for 'plugging' an electrode into GOD. Gooding and coworkers [30] also reported protein electrochemistry using aligned single walled carbon nanotube arrays. The process provides a simple method for covalently attaching enzymes onto carbon nanotube arrays on gold surface and opens a new avenue to detect biomolecules that interact with a linked enzyme by incorporating such structures in microfluidic devices. In this paper, the primary objective is to develop a microfluidic bioelectrochemical biochip by integrating enzyme molecules to an anchored SWCNT array architecture for electrochemical glucose detection.

2. MICROFABRICATION

2.1 Micropatterning

Glass wafers ($6 \times 6 \text{ cm}^2$) were cleaned with a piranha solution to remove any organic contamination and then rinsed thoroughly in Milli Q water before being blow dried using a clean nitrogen flow. The cleaned wafers were then spin coated with a $250 \text{ }\mu\text{m}$ thickness of SU-8 2025 negative photoresist (Micro Chem, USA) layer. After a pre-baking process, the coated wafers were then exposed to UV light through a photo mask (Circuit Graphics, UK) using a mask aligner (MJB3, Karl Suss). The exposed SU-8 2025 was then put through a post baking process before being developed in a developer solution (MicropositTM remover 1165, Rohm and HAAS Electronic Materials) to remove the unexposed regions of the SU-8 film, leaving a micropattern of the SU-8 structures on the glass wafers with characteristic dimensions of $250 \text{ }\mu\text{m}$ (height) by $500 \text{ }\mu\text{m}$ (width) by 4 cm (length). Using a soft lithography approach the raised SU-8 features were used as a micromould pattern to cast a microchannel in a polydimethylsiloxane (PDMS, Sylgard[®] 184 Silicone elastomer, Dow Corning).

2.2 Microelectrode fabrication

Using the photolithographic procedure as detailed in the previous section, positive photoresist MicropositTM S1828TM G2 (Rohm and HAAS Electronic Materials) was patterned on the surface of the glass wafers. After developing in MicropositTM 351 developer (Rohm and HAAS Electronic Materials), the patterned wafers were then put through a metal coating cycle using a metal evaporator (BOC Edwards Auto 306) to give a titanium (99.6%, Advent Research Materials Inc. UK) first then gold (99.99%, Advent Research Materials Inc. UK) film with a total thickness of approximately 200 nm . The electrode thickness proved sufficient not to require resistance compensation in the electrochemical measurements. The coated wafers were then immersed in acetone to lift off photoresist

to reveal the pattern of microelectrodes on the glass wafers. Then the working electrodes 1 and 2 (WE1 and WE2) were electrochemically plated with a thin layer of platinum using platinum P-salt aqueous slurry (Johnson Matthey, the UK) for better electrochemical catalysis activation. The default parameter settings for electrochemical devices were as follows: width of narrow electrode bands (ie, reference and working electrodes) is 500 μm ; width of broad electrode bands (ie, enzyme and counter electrodes) is 5000 μm ; default gap between enzyme electrode and the WE2 is 1800 μm ; gap between other bands is 30 μm .

2.3 Immobilisation of enzyme onto electrode band

DC arc discharge synthesized SWCNTs (P2-SWCNT, Carbon Solutions Inc., diameter 1.4 – 1.6 nm, length 0.5 – 1.5 μm) were purchased and functionalised for 8 hours in the mixed acid of concentrated HNO_3 and H_2SO_4 (1:3 by volume) using the previous method reported by Shapter [30, 34-38] and Liu [39, 40]. 0.020 g of functionalised SWCNTs and 0.100g of dicyclohexylcarbodiimide (DCC, $\geq 99\%$, Fluka) were dispersed in 200 mL of N, N-dimethylformamide (DMF, HPLC grade, 99.9+%, Aldrich) by ultrasonication for 5 hours to make a homogeneous SWCNTs/DMF suspension.

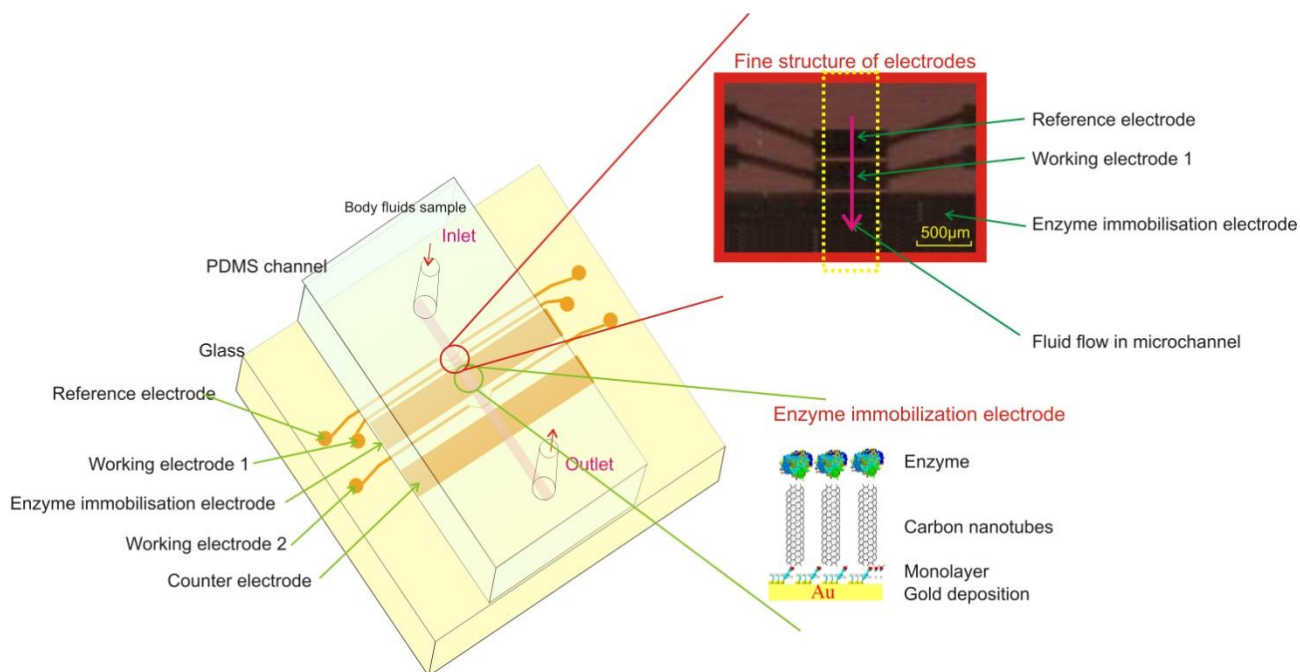


Figure 1. Schematic assembly of microfluidic device.

A clean enzyme microelectrode band fabricated through the Section 2.2 was exposed in a 0.2 mol L^{-1} cysteamine, ($\text{NH}_2(\text{CH}_2)_2\text{SH}$) / ethanol solution via a PDMS channel running parallel to the electrode band for 5 hours resulting in an amino terminated monolayer being formed. The use of the channel ensured that the rest of microelectrode bands were not exposed to the cysteamine solution. The microelectrodes were then washed with absolute ethanol and dried under nitrogen before being exposed to the SWCNTs/DMF suspension for 12 hours, allowing the amines on the gold surface to

form single-walled carbon nanotube arrays on gold (SWCNTs/Au array) via amide bonds [41]. After the condensation reaction had taken place, the PDMS channel was removed and thoroughly washed in Milli Q water, hydrolysing any remaining carbodiimide esters on the nanotube.

The terminal carboxylic acid groups of SWCNTs/Au array were activated by exposure to a pH 5.5 phosphate buffer solution (PBS) containing 0.02 mol L^{-1} N-(3-dimethylaminopropyl)-N'-ethylcarbodiimide hydrochloride (EDC, $\geq 99.0\%$, Fluka) and 0.05 mol L^{-1} N-hydroxysuccinimide (NHS, 98%, Aldrich) for 1 hour. The activated microelectrode band was rinsed with pH 5.5 PBS buffer solution and immediately placed in pH 5.5 PBS buffer solution with glucose oxidase ($490 \mu\text{g protein mL}^{-1}$, Type VII from *Aspergillus Niger*, EC 1.1.3.4, Sigma, UK) for 90 minutes. Microelectrodes with immobilised GOD were rinsed with copious amount of water and used immediately. The PDMS microchannel and enzyme immobilised microelectrode wafer were aligned as shown in Figure 1 before being joined and sealed by a clamp.

3. EXPERIMENTAL SETTINGS

Phosphate buffer solution containing one tablet of phosphate buffered saline (Sigma, UK) dissolved in 200 mL Milli Q water was adjusted to expected pH values using hydrochloric acid or potassium hydroxide to yield 0.01 mol L^{-1} phosphate buffer, $0.0027 \text{ mol L}^{-1}$ potassium chloride and 0.137 mol L^{-1} sodium chloride. D-(+)-glucose ($\geq 99.5\%$, Sigma, UK) stock solution (1 mol L^{-1}) was stored at $4 \text{ }^\circ\text{C}$. Other chemicals were of highest quality commercially available and were used without further purification. All aqueous solutions were prepared with Milli Q water. Phosphate buffer solution (pH = 7.0) containing $100 \mu\text{mol L}^{-1}$ ferrocenecarboxylic acid (FCA, 97%, Aldrich) was injected from the inlet and subsequently flowed through a microchannel over the reference electrode (a gold band was used as the pseudo reference electrode), WE1, enzyme electrode, WE2 and counter electrode in order. Glucose was added from the deoxygenated stock solution. Potential control was achieved by using a computer controlled homemade bi-potentiostat. Fluid motion was maintained with a programmable PHD 2000 syringe pump (Harvard Apparatus, USA). All experiments were conducted at $20 \text{ }^\circ\text{C}$. The concentration profiles in microchannels were simulated using a finite difference model as reported previously [42].

4. RESULTS AND DISCUSSION

4.1 Geometry optimization for working electrodes

To optimise the geometry of working electrodes, we used the WE1 while WE2 was not connected. A series of linear sweep voltammograms on the WE1 (as shown in Figure 2a) were taken from 0.01 mol L^{-1} phosphate buffer solution (pH = 7.0) containing $100 \mu\text{mol L}^{-1}$ ferrocenecarboxylic acid for the flow rate range from 0 to 0.5 mL min^{-1} . Plot of limiting current against the cube root of volume flow rate is found to be linear in the flow range of 0.005 to 0.5 mL min^{-1} , in accordance with the Levich equation [43-45], as shown in the inset of Figure 2(a).

$$I_{\text{lim}} = 0.925nFw[C]_{\text{bulk}}(x_e D)^{2/3} \left(\frac{V_f}{h^2 d}\right)^{1/3} \quad (4)$$

where n is the number of electrons transferred in the half reaction, F is the Faraday constant, and $[C]_{\text{bulk}}$ is the bulk concentration of analyte, V_f is the volume flow rate, D is the diffusion coefficient, and the other terms represent the geometry of the channel cell and electrode. In detail, x_e the length of the electrode (in the direction of flow), h the half-height of the cell, d the channel width and w the electrode width. The gradient of this plot can be used to obtain a value for the diffusion coefficient of ferrocenecarboxylic acid by application of the Levich equation. The value is estimated as $6.85 \times 10^{-6} \text{ cm}^2 \text{ s}^{-1}$, which is very close to the reported diffusion coefficient $4.96 \times 10^{-6} \text{ cm}^2 \text{ s}^{-1}$ [46]. Linear sweep voltammograms for different widths of working electrode bands are compared in Figure 2(b), taken from 0.01 mol L^{-1} phosphate buffer solution ($\text{pH} = 7.0$) containing $100 \mu\text{mol L}^{-1}$ ferrocenecarboxylic acid. For a $100 \mu\text{m}$ wide electrode band, the limiting current is about $0.118 \mu\text{A}$ while the limiting current becomes about $0.174 \mu\text{A}$ for a $200 \mu\text{m}$ wide electrode, an additional increase of about 47%. A width of $500 \mu\text{m}$ gives a limiting current of $0.190 \mu\text{A}$, a further increase of about 9 % in comparison to the $200 \mu\text{m}$ wide band. While an increase to an electrode width of $1000 \mu\text{m}$ yields a limiting current about $0.198 \mu\text{A}$, only an extra increase of 4% compared to the $500 \mu\text{m}$ band. It is clear that an increase in the width of electrode band leads to a higher limiting current. However the limiting current does not reach a maximum for electrode width of about 1 mm. A similar result has been reported by Henley and his co-workers [47] based on the digital simulation of voltammetry in microchannels through finite element technique. They found that the current density drops in region close to the leading edge because of the hydrodynamic boundary layer. Since a further increase of band width does not improve the current response significantly, $500 \mu\text{m}$ was chosen for both working electrodes (WE1 and WE2) in the rest of this work.

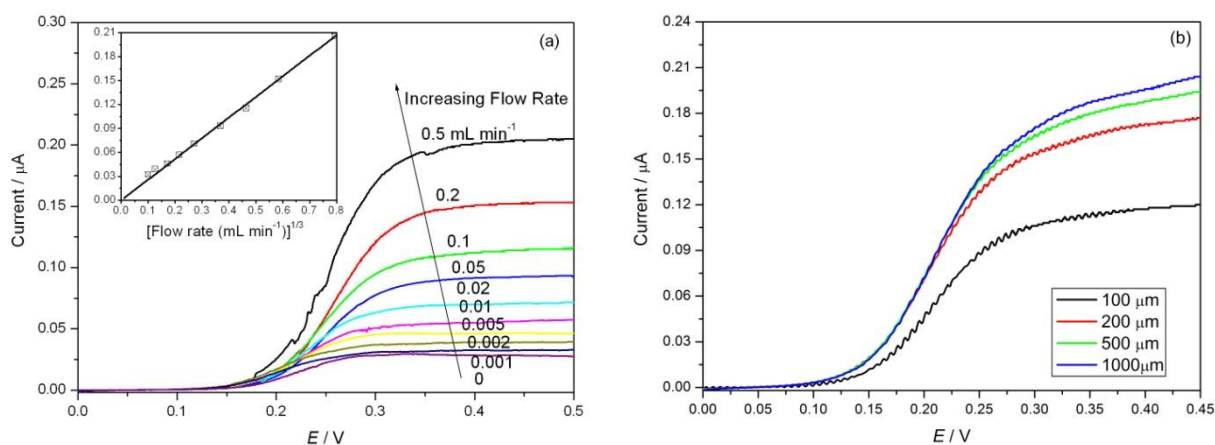


Figure 2. (a) Linear sweep voltammograms on the WE1 taken from 0.01 mol L^{-1} phosphate buffer solution ($\text{pH} = 7.0$) containing $100 \mu\text{mol L}^{-1}$ ferrocenecarboxylic acid at potential scan rate 5 mV s^{-1} . Inset: Limiting currents plotted as a function of flow rate. (b) Linear sweep voltammograms on the WE1 in the same solution for different widths of working electrode bands at flow rate 0.5 mL min^{-1} and potential scan rate 5 mV s^{-1} .

4.2 Immobilisation of glucose oxidase

Linear sweep voltammograms were taken from 0.01 mol L⁻¹ phosphate buffer solution (pH = 7.0) containing 100 μmol L⁻¹ ferrocenecarboxylic acid and 2 mmol L⁻¹ D-(+)-glucose when no glucose oxidase is present. The potential sweeps on the WE1 started from 0 V for all flow rates, going in the anodic direction, while the potential on the WE2 is held constant at 0.6 V for all experiments. When glucose oxidase is absent, linear sweep voltammograms taken from 0.01 mol L⁻¹ phosphate buffer solution (pH = 7.0) containing 100 μmol L⁻¹ ferrocenecarboxylic acid 2 mmol L⁻¹ D-(+)-glucose are shown in Figure 3(a). At the typical flow rate of 0.5 mL min⁻¹, the current response on the WE1 is small at the beginning, nearly zero. Meanwhile the current response on the WE2 is the maximum observed, about 0.205 μA. After the potential sweep on the WE1 attains 0.2 V, its current response starts to increase while the current on the WE2 goes down. When the potential on the WE1 reaches 0.60 V, its current response reaches a maximum, about 0.203 μA, while the current response on the WE2 reaches a minimum, about 0.159 μA. After glucose oxidase is immobilised, the comparison of linear sweep voltammograms taken from the same solution is shown in Figure 3(b). Typically at a flow rate of 0.5 mL min⁻¹, the current response on the WE2 is a maximum, about 0.203 μA, at the beginning of potential sweep on the WE1. After the potential sweep on the WE1 attains 0.45 V, its current response reaches a maximum of about 0.204 μA while the current response on the WE2 reaches a minimum, about 0.174 μA. By comparing the current responses for both presence and absence of enzyme, the maximum current response on the WE1 and WE2 are similar. However, the minimum current response on the WE2 is much higher when the presence of enzyme.

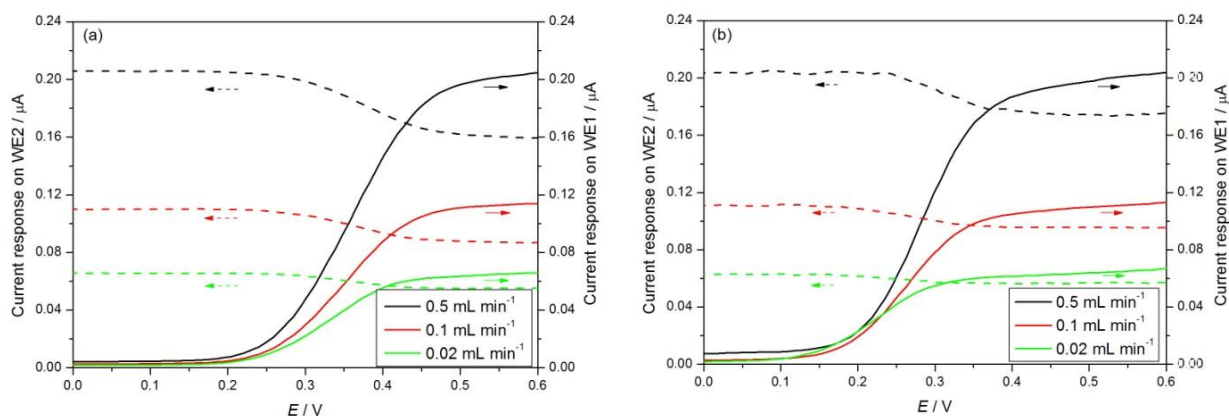


Figure 3. Comparison of linear sweep voltammograms taken from 0.01 mol L⁻¹ phosphate buffer solution (pH = 7.0) containing 100 μmol L⁻¹ ferrocenecarboxylic acid 2 mmol L⁻¹ D-(+)-glucose when glucose oxidase is absent (a) and present (b). The potential on WE1 was scanned from 0 to 0.6 V at scan rate 5 mV s⁻¹, while the potential on WE2 was held constant at +0.6 V. Solid line: Current response on the WE1. Dash line: Current response on the WE2.

The possible chemical reactions that occur in microchannels are shown in Figure 4 (a) when enzyme is absent. Ferrocenecarboxylic acid molecules are first oxidised on the WE1, then flow over the enzyme electrode. No reaction takes place between FCA⁺ and glucose. The simulated FCA

concentration profile is shown in Figure 5(a), indicating an immediate FCA concentration drop close to the WE1 region. The FCA concentration drop consequently results in the diffusion of FCA from laminar layers further from the electrode to compensate the concentration consumption. So it can be seen that the FCA concentration alongside the electrodes surface gradually recovers (as shown in Figure 5c). However the local concentration of FCA has not relaxed enough to reach its bulk concentration level when the fluid passes over the WE2. So it is not surprising to see a reduced current response on the WE2.

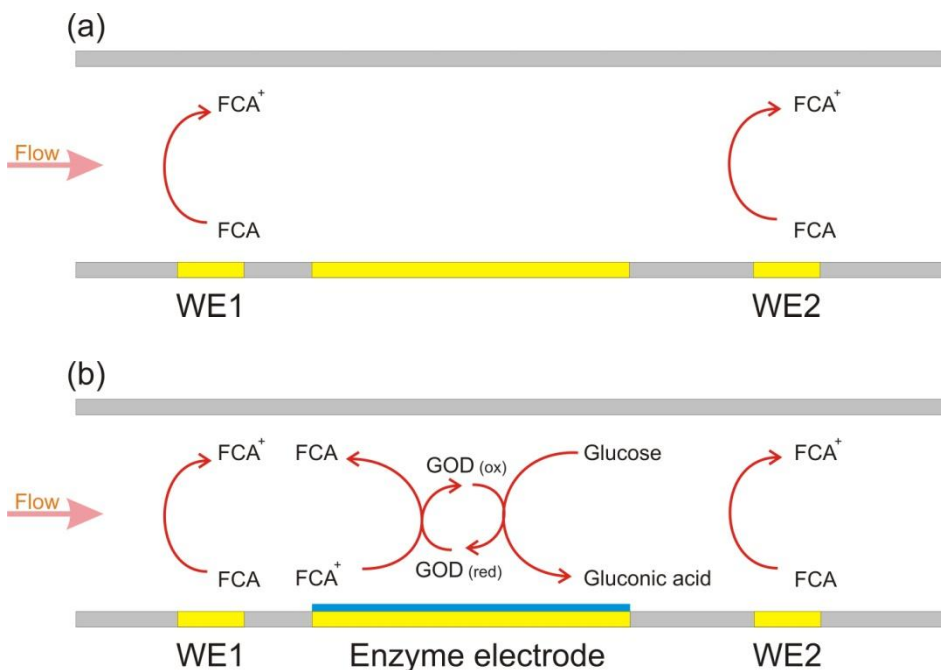


Figure 4. Comparison of possible chemical reactions in microchannels when enzyme is absent (a) and present (b).

When enzyme is present, the possible chemical reactions that occur in microchannels are shown in Figure 4 (b). The oxidation product (FCA⁺) on the WE1 flows over the enzyme electrode, and quickly reacts with GOD_{red} to give FCA and GOD_{ox}. The GOD_{ox} then oxidises glucose to generate gluconic acid. So the concentration of FCA promptly recovers to the bulk concentration level. A higher current response on the WE2 is observed as shown in Figure 5 (b). For a better comparison, the simulated FCA concentration profiles alongside the electrodes surface are shown for both presence and absence of enzyme in Figure 5 (c). With the absence of enzyme, the surface concentration of FCA sharply drops down on the WE1 and gradually rises owing to the bulk diffusion of FCA in the channel. However it recovers more rapidly with the catalysis of enzyme. A higher current response is expected with the presence of enzyme, just as experimental observation in Figure 3 (b), when the fluid flows over the WE2. Therefore the results indicate that with the application of glucose oxidase, the concentration of glucose could be successfully determined by examining the current response on the WE2. It is worth noting that a small surface concentration drop is observed in Figure 5(c) with the

presence of enzyme when the fluid flows away from the enzyme electrode. However a similar drop does not appear with the absence of enzyme. So the surface concentration drop is very likely attributed to the FCA diffusion from the surface to further laminar layers due to a quick turnover of FCA with the presence of enzyme. According to the Equation 4, the surface concentration drop will reduce the current response on the WE2 and lower the detection sensitivity of our microfluidic devices. Therefore it is very important to experimentally study the effects of electrode gap on current responses.

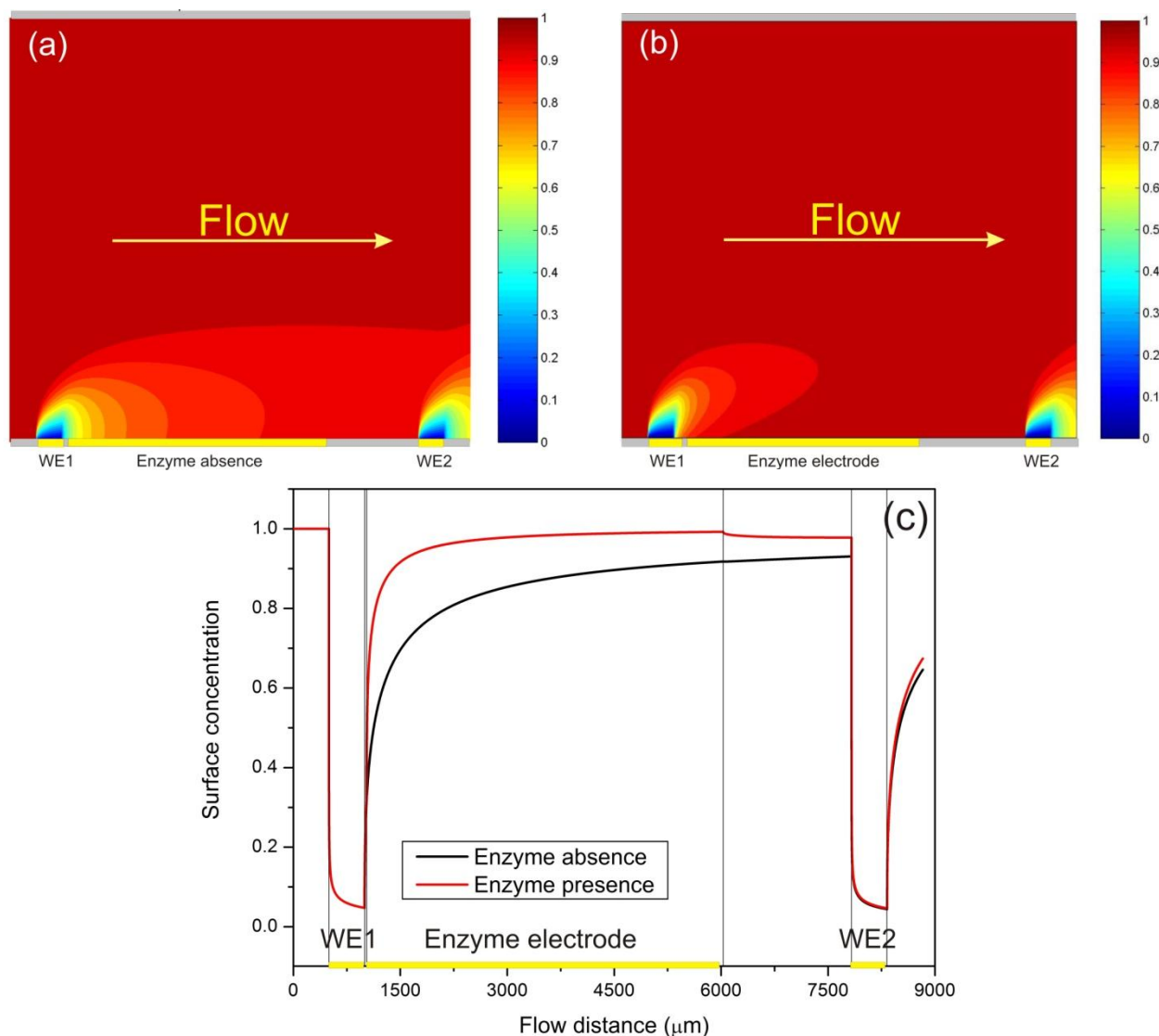


Figure 5. Simulated FCA concentration profiles in microchannels with the absence (a) and presence (b) of enzyme when the potential on both WE1 and WE2 is held at 0.6 V. (c) The comparison of simulated FCA concentration profiles at electrodes surface. Parameters used by the simulations are flow rate = $0.02 \text{ mL}\cdot\text{min}^{-1}$, electrode gap = $1800 \text{ }\mu\text{m}$, $D=5.7\times 10^{-6} \text{ cm}^2 \text{ s}^{-1}$ and the kinetic rate constant of reaction between FCA^+ and $\text{GOD}_{(\text{red})}$ $k_{\text{Equation } 2}=9\times 10^8 \text{ mol}^{-1} \text{ cm}^3 \text{ s}^{-1}$. Other parameters are the same as the default settings.

4.3 Effects of electrode gap on current response

The electrode gap between the enzyme electrode and WE2 was reduced to 30 μm from 1800 μm .

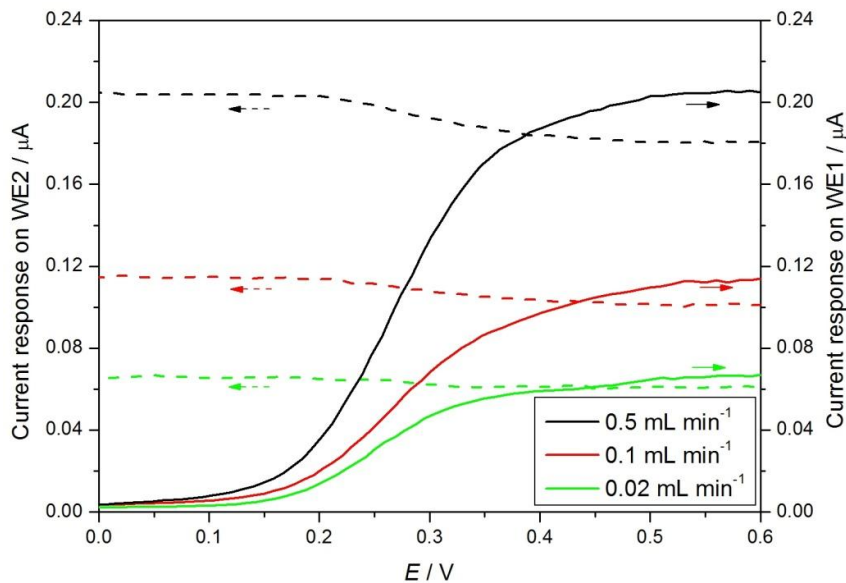


Figure 6. Linear sweep voltammograms taken from 0.01 mol L⁻¹ phosphate buffer solution (pH = 7.0) containing 100 $\mu\text{mol L}^{-1}$ ferrocenecarboxylic acid and 2 mmol L⁻¹ D-(+)-glucose when glucose oxidase is present. The potential on the WE1 was scanned from 0 to 0.6 V at scan rate 5 mV s⁻¹, and the potential on the WE2 was held constant at +0.6 V. Solid line: Current response on the WE1. Dash line: Current response on the WE2.

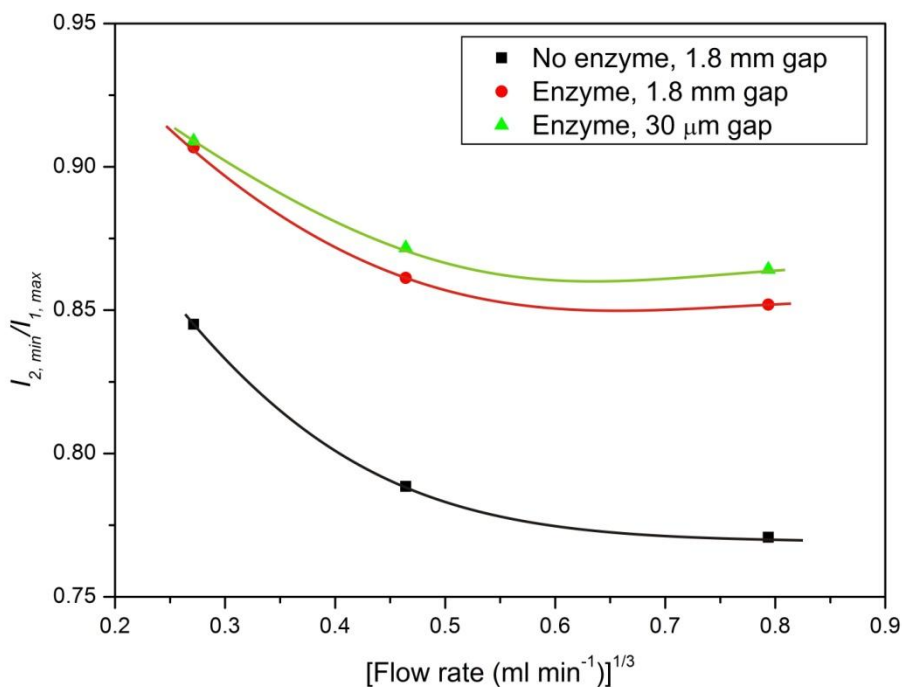


Figure 7. Plot of $I_{2, min} / I_{1, max}$ against the cube root of volume flow rate for 30 μm and 1800 μm gap when the presence and absence of enzyme.

Figure 6 shows the linear sweep voltammograms taken from 0.01 mol L⁻¹ phosphate buffer solution (pH = 7.0) containing 100 μmol L⁻¹ ferrocenecarboxylic acid and 2 mmol L⁻¹ D-(+)-glucose when glucose oxidase is present. Under the flow rate of 0.5 mL min⁻¹, the current response on the WE2 reaches a maximum about 0.205 μA at the beginning of potential sweep, which keeps reasonably the same as the current before the geometry changes. After the potential sweep on the WE1 reaches 0.45 V, the current response on the WE2 reaches a minimum, about 0.180 μA. Compared to the current response, 0.170 μA, for a bigger electrode gap of 1800 μm, the minimum current response for a smaller electrode gap of 30 μm is greater. The maximum current on the WE1 and minimum current on the WE2 are denoted as $I_{1,max}$ and $I_{2,min}$ respectively, therefore the ratio of $I_{2,min}/I_{1,max}$ against the cube root of volume flow rate is plotted in Figure 7 for different electrode gaps when the absence and presence of enzyme. It can be seen that the device with 30 μm gap produces the highest $I_{2,min}/I_{1,max}$ value at a given flow rate when the presence of enzyme.

4.4 Microfluidic devices for glucose detection

Since the $I_{1,max}$ and $I_{2,min}$ are the current values observed for both working electrodes at the potential of 0.6 V, to be a real microfluidic device for glucose detection in practical uses, the glucose detection is simplified to monitor current values through both WE1 and WE2 by holding their electrode potential constant at 0.6 V. The two current values are denoted as I_1 on the WE1 and I_2 on the WE2 respectively, the variation of I_2/I_1 against the glucose concentration is shown in Figure 8. The variation in current response is reasonably linear up to a glucose concentration of 5 mmol L⁻¹, where the square of the correlation coefficient is 0.9509.

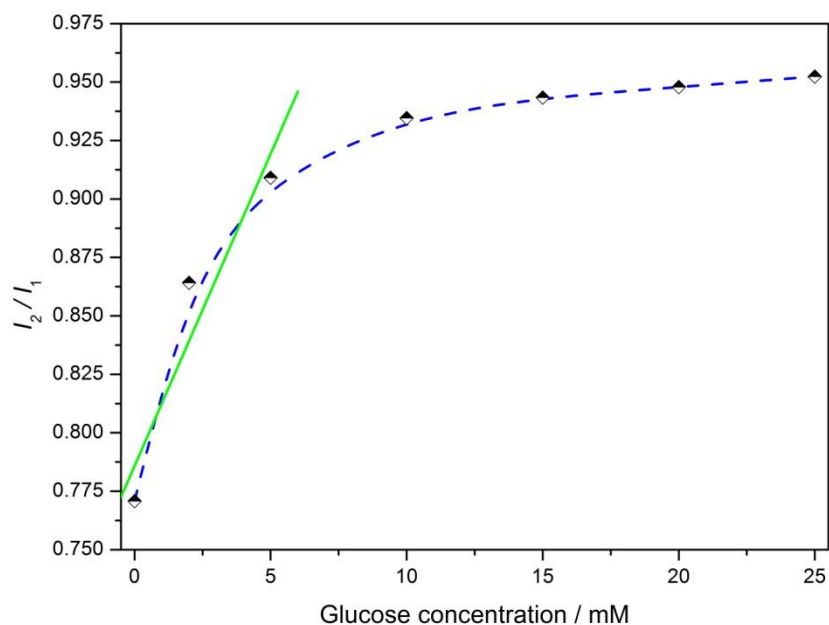


Figure 8. The variation of I_2/I_1 ratio against the concentration of glucose.

Similarly, Chen and co-workers [11] reported the fabrication of tube-like microchannels made of UV curable polymer on a glass substrate and the device assembling with a disposable enzyme-working electrode for high-sensitivity electrochemical detection. Using glucose oxidase-coated gold electrodes, they were able to determine a linear amperometry response to the glucose concentrations in the range of 2 – 16 mmol L⁻¹. Ju and co-workers [48] reported a microfluidic device for amperometric determination of glucose by packing enzyme modified magnetic nanoparticles (MNPs) in its microchannel as an enzyme microreactor. Glucose oxidase was covalently attached to the surface of MNPs and localized in the microchannel by the help of an external magnetic field, leading to a tuneable packing length. By changing the length of microreactor from 3 to 10 mm, the performance for glucose detection was optimized. The optimal linear range to glucose was from 25 μmol L⁻¹ to 15 mmol L⁻¹ with a detection limit of 11 μmol L⁻¹ at a length of 6 mm. Compared to these reported microfluidic devices, our linear range could be extended by changing configuration parameters of microfluidic devices, such as the width of enzyme electrode, electrode gap between detecting electrode and enzyme electrode as well as the dimensions of microchannel. Actually, the sensitivity and dynamic range of our microfluidic devices is similar to a multilayer enzyme electrode [49] and channel sensor [6] despite the much smaller amount of enzyme immobilised. Also the devices reported in this paper have a higher detection sensitivity and some advantages such as the simple design and low cost, in comparison with the approach of employing both horseradish peroxidase and glucose oxidase immobilised single walled carbon nanotube matrix in microchannels [7]. Because of small amounts of fluids and enzyme in microchannels, microfluidic technologies offer a number of technical advantages, such as minimal device size for hand-held instrumentation and point-of-care testing, low production costs per device allowing disposable microfluidic systems, precise volumetric control of samples and reagents leading to higher sensitivities in analytical applications and efficient use of expensive chemical reagents.

5. CONCLUSIONS

Microfluidic devices for glucose detection have been constructed and developed by integration of glucose oxidase functionalised carbon nanotube arrays into a poly (dimethylsiloxane)-based microfluidic channel. The enzymes were covalently attached to the ends of the aligned carbon nanotubes by modifying single walled carbon nanotubes connected to a cysteamine self-assembled monolayer on gold electrodes. In the presence of the catalyst glucose oxidase, FCA⁺ ions can be turned over to FCA molecules when a glucose solution containing ferrocenecarboxylic acid flowed down the microchannel allowing the detection of the presence of glucose. The electrochemical results showed that the glucose can be detected with a linear response up to 5 mmol L⁻¹ glucose concentration. The influence of parameters such as flow rate, width of working electrode and the gap between the enzyme layer and the detector electrode were also explored.

ACKNOWLEDGEMENTS

The financial support of this work by the Australian Research Council (Project No DP0985176) is gratefully acknowledged. Yu would like to acknowledge the travel support from the Roger Pysden Memorial Fellowship, ARCNN Overseas Travel Fellowship, ARNAM Scholarship for Collaborative Research Support and a Flinders University Overseas Traveling Grant.

References

1. P.-E. Paulev, Textbook in medical physiology and pathophysiology: Essentials and clinical problems, Copenhagen Medical Publishers, Copenhagen, 1999.
2. F. Prisco, A. Picardi, D. Iafusco, R. Lorini, L. Minicucci, M.E. Martinucci, S. Toni, F. Cerutti, I. Rabbone, R. Buzzetti, A. Crino, P. Pozzilli, *Pediatr. Diabetes*, 7 (2006) 223-228.
3. H. Gunasingham, C.H. Tan, H.M. Ng, *J Electroanal Chem*, 287 (1990) 349-362.
4. W.Z. Jia, K. Wang, Z.J. Zhu, H.T. Song, X.H. Xia, *Langmuir*, 23 (2007) 11896-11900.
5. Y. Wang, Q.H. He, Y.Y. Dong, H.W. Chen, *Sensor Actuat B-Chem*, 145 (2010) 553-560.
6. D. Losic, M. Zhao, J.G. Shapter, J.J. Gooding, *Electroanal*, 15 (2003) 183-190.
7. J. Kim, J. Baek, H. Kim, K. Lee, S. Lee, *Sens. Actuator A-Phys.*, 128 (2006) 7-13.
8. K.L. Brown, J.S. Pinter, K.L. Ewing, T.R. Ruch, M. Ambrose, I. Hesslesweet, *Anal. Lett.*, 38 (2005) 769-780.
9. I.A. Ges, F. Baudenbacher, *Biosens. Bioelectron.*, 25 (2010) 1019-1024.
10. N.P. Rodrigues, Y. Sakai, T. Fujii, *Sensor Actuat B-Chem*, 132 (2008) 608-613.
11. X. Li, F. Zhang, J. Shi, L. Wang, J.-H. Tian, X.-T. Zhou, L.-M. Jiang, L. Liu, Z.-J. Zhao, P.-G. He, Y. Chen, *Electrophoresis*, 32 (2011) 3201-3206.
12. S. Marxtibbon, E. Katz, I. Willner, *Journal of the American Chemical Society*, 117 (1995) 9925-9926.
13. J. Wang, *Chem Rev*, 108 (2008) 814-825.
14. A.V. Barmin, A.V. Eremenko, I.N. Kurochkin, A.A. Sokolovsky, *Electroanal*, 6 (1994) 107-112.
15. C. Mousty, C. Forano, S. Fleutot, J.C. Dupin, *Electroanal*, 21 (2009) 399-408.
16. M.E. Ghica, C.M.A. Brett, *Anal. Lett.*, 38 (2005) 907-920.
17. M.G. Boutelle, L.K. Fellows, C. Cook, *Analytical Chemistry*, 64 (1992) 1790-1794.
18. F.K. Balagadde, L.C. You, C.L. Hansen, F.H. Arnold, S.R. Quake, *Science*, 309 (2005) 137-140.
19. G.M. Whitesides, *Nature*, 442 (2006) 368-373.
20. Y.J. Liu, S.S. Guo, Z.L. Zhang, W.H. Huang, D.M. Baigl, Y. Chen, D.W. Pang, *J Appl Phys*, 102 (2007) 6.
21. H. Song, R.F. Ismagilov, *Journal of the American Chemical Society*, 125 (2003) 14613-14619.
22. M.W. Losey, R.J. Jackman, S.L. Firebaugh, M.A. Schmidt, K.F. Jensen, *J. Microelectromech. Syst.*, 11 (2002) 709-717.
23. S. Cho, D.K. Kang, J. Choo, A.J. deMello, S.I. Chang, *BMB Rep.*, 44 (2011) 705-712.
24. B. Mosadegh, T. Bersano-Begey, J.Y. Park, M.A. Burns, S. Takayama, *Lab Chip*, 11 (2011) 2813-2818.
25. S. Iijima, T. Ichihashi, *Nature*, 363 (1993) 603-605.
26. C. Gouveia-Caridade, R. Pauliukaite, C.M.A. Brett, *Electrochim Acta*, 53 (2008) 6732-6739.
27. Y.H. Yun, Z.G. Dong, V.N. Shanov, M.J. Schulz, *Nanotechnology*, 18 (2007).
28. A.G. Crevillen, M. Avila, M. Pumera, M.C. Gonzalez, A. Escarpa, *Analytical Chemistry*, 79 (2007) 7408-7415.
29. J.Q. Liu, A. Chou, W. Rahmat, M.N. Paddon-Row, J.J. Gooding, *Electroanal*, 17 (2005) 38-46.
30. J.J. Gooding, R. Wibowo, J.Q. Liu, W.R. Yang, D. Losic, S. Orbons, F.J. Mearns, J.G. Shapter, D.B. Hibbert, *Journal of the American Chemical Society*, 125 (2003) 9006-9007.
31. F. Patolsky, Y. Weizmann, I. Willner, *Angew Chem Int Edit*, 43 (2004) 2113-2117.

32. J. Seo, T.J. Lee, S. Ko, H. Yeo, S. Kim, T. Noh, S. Song, M.M. Sung, H. Lee, *Adv Mater*, 24 (2012) 1975-1979.
33. D. Vilela, A. Anson-Casaos, M. Teresa Martinez, M. Cristina Gonzalez, A. Escarpa, *Lab Chip*, 12 (2012) 2006-2014.
34. J.X. Yu, D. Losic, M. Marshall, T. Bocking, J.J. Gooding, J.G. Shapter, *Soft Matter*, 2 (2006) 1081-1088.
35. J.X. Yu, J.G. Shapter, J.S. Quinton, M.R. Johnston, D.A. Beattie, *Physical Chemistry Chemical Physics*, 9 (2007) 510-520.
36. B.S. Flavel, J.X. Yu, J.G. Shapter, J.S. Quinton, *Electrochim Acta*, 53 (2008) 5653-5659.
37. J.X. Yu, S. Mathew, B.S. Flavel, M.R. Johnston, J.G. Shapter, *Journal of the American Chemical Society*, 130 (2008) 8788-8796.
38. J. Yu, O. Zvarec, D.M. Huang, M.A. Bissett, D.B. Scanlon, J.G. Shapter, A.D. Abell, *Chem Commun*, 48 (2012) 1132-1134.
39. X.L. Nan, Z.N. Gu, Z.F. Liu, *J. Colloid Interface Sci.*, 245 (2002) 311-318.
40. Z.F. Liu, Z.Y. Shen, T. Zhu, S.F. Hou, L.Z. Ying, Z.J. Shi, Z.N. Gu, *Langmuir*, 16 (2000) 3569-3573.
41. K.E. Moore, B.S. Flavel, J. Yu, A.D. Abell, J.G. Shapter, *Electrochim Acta*, 89 (2013) 206-211.
42. A.G. Deshpande, Y.F. Gu, S.M. Matthews, K. Yunus, N.K.H. Slater, C.M. Brennan, A.C. Fisher, *Chemical Engineering Journal*, 149 (2009) 428-434.
43. N.V. Rees, O.V. Klymenko, B.A. Coles, R.G. Compton, *J Electroanal Chem*, 534 (2002) 151-161.
44. J.A. Cooper, R.G. Compton, *Electroanal*, 10 (1998) 141-155.
45. J. Booth, R.G. Compton, J.A. Cooper, R.A.W. Dryfe, A.C. Fisher, C.L. Davies, M.K. Walters, *J Phys Chem-Us*, 99 (1995) 10942-10947.
46. R. Antiochia, I. Lavagnini, F. Magno, *Electroanal*, 11 (1999) 129-133.
47. I.E. Henley, K. Yunus, A.C. Fisher, *J Phys Chem B*, 107 (2003) 3878-3884.
48. J. Sheng, L. Zhang, J.P. Lei, H.X. Ju, *Anal Chim Acta*, 709 (2012) 41-46
49. J.J. Gooding, P. Erokhin, D.B. Hibbert, *Biosens. Bioelectron.*, 15 (2000) 229-239